Journal of Alloys and Compounds 482 (2009) 502–507

Contents lists available at ScienceDirect

Journal of Alloys and Compounds

journal homepage: www.elsevier.com/locate/jallcom

Thermal stability and crystallization of $Fe_{89.8}Ni_{1.5}Si_{5.2}B_3C_{0.5}$ amorphous alloy

D.M. Minić[a,*], A. Gavrilović[b], P. Angerer[b], D.G. Minić[c], A. Maričić[c]

[a] Faculty of Physical Chemistry, University of Belgrade, Studentski trg 12, 11001 Belgrade, Serbia
[b] CEST Kompetenzzentrum für Elektrochemische Oberflächentechnologie GmbH, Viktor-Kaplan-Strasse 2, A-2700 Wiener Neustadt, Austria
[c] Technical Faculty of Čačak, University in Kragujevac, Svetog Save 65, 32000 Čačak, Serbia

ARTICLE INFO

Article history:
Received 9 February 2009
Received in revised form 9 April 2009
Accepted 14 April 2009
Available online 21 April 2009

Keywords:
Metallic glasses
Differential thermal analysis (DTA)
X-ray diffraction (XRD)
Phase transformations

ABSTRACT

The thermal stability and crystallization of the $Fe_{89.8}Ni_{1.5}Si_{5.2}B_3C_{0.5}$ amorphous alloy in non-isothermal as well as in isothermal conditions were studied. It was shown that the amorphous alloy was stable up to a temperature of 753 K when a multi-step structural transformation began. Initially an α-Fe phase was formed, followed by a Fe_2B phase at temperatures over 813 K. Kinetic parameters, the activation energy (E_a) and the pre-exponential factor ($\ln A$), for both crystallization steps were determined as $E_a = 486.3\ kJ\ mol^{-1}$ and $\ln A$ (A [min^{-1}]) = 72.7 for first step and $E_a = 446.3\ kJ\ mol^{-1}$ and $\ln A$ (A [min^{-1}]) = 63.7 for second step according the Kissinger method and as $E_a = 499.9\ kJ\ mol^{-1}$ and $\ln A$ (A [min^{-1}]) = 88.1 for first step and $E_a = 460.8\ kJ\ mol^{-1}$ and $\ln A$ (A [min^{-1}]) = 79.2 for second step according the Ozawa method.

1. Introduction

Disordered structural arrangement of Fe-based amorphous alloys have been a subject of considerable scientific interest because of their soft ferromagnetic properties, good mechanical properties and high corrosion resistance making them very useful in a variety of devices including the transformers, sensors, magnetic tapes, recorder heads, microgears, welding elements as well as dental and medical implants [1,2]. However, the application of Fe-based amorphous alloys as structural materials is limited because of the very high cooling rates required for their production to avoid crystallization and high vacuum to overcome oxidation. The improving of the purity of starting materials or the addition of metalloids such as B, P, Si or C enhances the glass-forming ability of these materials [3,4]. The substitution of Fe by Co, Ni or Co and Ni, as well as increasing B/Si concentration ratio largely increases of the glass-forming ability of Fe-based amorphous alloy, too. The amorphous alloys are metastable materials so that the elevated temperature as well as the prolonged performance could induce their transformation into a crystalline state which, in turn deteriorates their advantageous physical properties [5]. However, suitable thermal treatment of amorphous alloys of an appropriate composition could produce nanocrystalline alloys whose magnetic parameters do not substantially deteriorate at elevated temperatures during their practical exploitation. Because of their technological applicability, the nanocrystalline Fe-based alloys possessing a metastable two-phase microstructure with outstanding soft magnetic properties, very low coercivity, high saturation magnetic flux and high permeability as a consequence of the averaging out of the magnetic anisotropy of the crystalline phase as the exchange length becomes larger than the structural length, are very interesting materials [6]. For these reasons the knowledge of the thermal stability and structural transformations of amorphous alloys is of great interest for two important reasons [7]. First, for amorphous alloys that exhibit excellent magnetic and electric properties the onset of crystallization represents the limit when these properties begin to deteriorate [8]. Second, control of the crystallization process gives us the ability to tailor the microstructure that provides the desired properties in nanocrystalline–amorphous matrix alloys [9–11]. On the other hand, the ability to predict and control of the crystallization process of amorphous alloys is very important for the preparation and preservation of useful microstructure. The detailed analysis of crystallization data can also provide important information about the temperature dependence of the processes of nucleation and the growth of the crystallites in order to get and control the optimal microstructure [12,13]. The crystallization of these materials upon heating can be performed in several ways. Usually, two basic methods are considered: isothermal and non-isothermal. In these cases several techniques, such as differential scanning calorimetry [14], X-ray scattering [15], measurement of electrical resistivity [16], and Mössbauer spectrometry [17] have been used to study crystallization of amorphous metallic alloys.

We have previously studied a series of amorphous alloys based on Fe and Co, from fundamental and practical points of view [18–21]. The present paper concerns studies of the thermal stability

* Corresponding author. Tel.: +381 11 3336 689.
E-mail address: dminic@ffh.bg.ac.yu (D.M. Minić).

0925-8388/$ – see front matter © 2009 Elsevier B.V. All rights reserved.
doi:10.1016/j.jallcom.2009.04.050

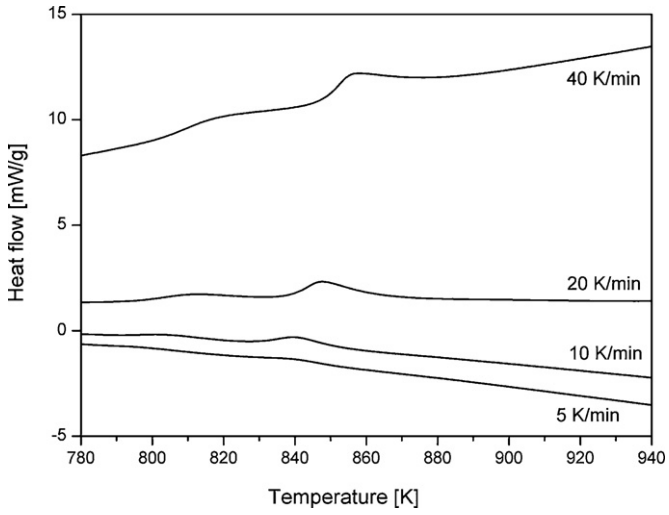

Fig. 1. DSC curves of the $Fe_{89.8}Ni_{1.5}Si_{5.2}B_3C_{0.5}$ sample recorded at heating rates of 5, 10, 20, 40 K/min, respectively.

and structural transformations of $Fe_{89.8}Ni_{1.5}Si_{5.2}B_3C_{0.5}$ amorphous alloy induced by heating over the temperature range 298–1123 K.

2. Experimental procedures

Ribbon shaped samples of $Fe_{89.8}Ni_{1.5}Si_{5.2}B_3C_{0.5}$ amorphous alloy with dimensions 2 cm wide and 35 μm thick were obtained using the standard procedure of rapid quenching of the melt on a rotating disc (melt-spinning method).

Thermal stability of the alloy as well as the structural transformations was investigated by differential scanning calorimetry (DSC) in a nitrogen atmosphere using a DSC-50 analyzer (Shimadzu, Japan). Samples weighting several milligrams were heated in the DSC cell from room temperature to 1123 K in a stream of nitrogen flowing at 20 mL min^{-1} and with constant heating rates of 5, 10, 20 and 40 K min^{-1}.

The X-ray diffraction (XRD) experiments were performed on an X-Pert powder diffractometer (PANalytical, Netherlands) using CuKα radiation in a Bragg-Brentano geometry at 40 kV and 30 mA. This device is equipped with a secondary graphite monochromator, automatic divergence slits, and a scintillation counter. The diffraction angle was changed stepwise in 0.05° (2θ) intervals with a measuring time of 30 s/step.

The Rietveld refinement method as well as the single peak refinement approach to analyze the XRD measurements was used. The TOPAS V3 general profile and structure analysis software for powder diffraction data was used for this purpose [22].

The Vickers microhardness tests were performed with a microhardness tester MHT-10 (Anton Paar, Austria) with loads of 0.4 N and 10 s loading time. For each sample multiple microhardness measurements were conducted.

For the scanning electron microscopy (SEM) investigations an XL 30 ESEM-FEG (Environmental Scanning Microscope with Field Emission Gun, by FEI, Netherlands) device was used. The samples were inspected using a 20 kV acceleration voltage at a magnification of 3500× and 20,000×.

3. Results and discussion

In Fig. 1 typical dynamic differential scanning calorimetry curves for the amorphous $Fe_{89.8}Ni_{1.5}Si_{5.2}B_3C_{0.5}$ alloy at four different heating rates (5, 10, 20 and 40 K min^{-1}) are displayed.

All DSC curves in the temperature range of 780–880 K show two well formed crystallization peaks indicating the multi-stage crystallization process of the alloy. The temperatures of both peaks increase with an increase of the heating rate, indicating the thermal activation of both steps of the crystallization process.

The apparent activation energy of crystallization E_a for each observed crystallization step as well as the frequency factor A for linear heating, can be determined by Kissinger's as well as Ozawa's peak method from the relationship between the exothermic peak temperature T_p and the heating rate β [23,24].

According to Kissinger [23] the apparent activation energy can be determined by applying the equation:

$$\ln\left(\frac{\beta}{T_p^2}\right) = \ln\left(\frac{AR}{E_a}\right) - \frac{E_a}{RT_p} \quad (1)$$

where plotting $\ln(\beta/T_p^2)$ as a function of $1/T_p$ yields a straight line with a slope of $-E_a/R$ and an intercept of $\ln(AR/E_a)$.

For the determination of the apparent activation energy under non-isothermal conditions Ozawa [24] proposed the equation:

$$\ln\beta = \ln\left(\frac{AE_a}{R}\right) - \frac{E_a}{RT_p} \quad (2)$$

where plotting of $\ln(\beta)$ versus $1/T_p$ yields a straight line with a slope of $-E_a/R$ and an intercept of $\ln(AE_a/R)$.

The values of the kinetic parameters determined according to the Kissinger method are some higher than ones determined by applying the Ozawa method, but the differences between the values determined by the two methods are under 3%. Errors in the calculated values were determined as a root-square deviation multiplied by Student's coefficient for a probability of 0.95 (Table 1).

In our experiments as well as for other amorphous alloys based on Fe [25,26] we found high values of the apparent activation energy of crystallization (cf. Table 1). The activation energy of solid state reactions proceeding through formation of nuclei and their growth, according to the opinion of some researchers, has only an empirical character and yields a practical determination of the dependence of the rate of conversion on temperature. This energy can be spent, not only for overcoming the activation barrier but also for lowering the activation barrier due to co-operative displacement of atoms. In these experiments, the total value of energy is determined both, for the lowering of the potential activation barrier and for overcoming the barrier. The high values of activation energy of crystallization of amorphous alloys indicates that a significant fraction of the atoms participate in the structural reorganization.

The amorphous structure of an alloy prepared by rapid quenching of the melt was tested by X-ray diffraction methods. To study the structural transformations induced by heating, samples of the alloy were isothermally treated at different temperatures between 573 and 1123 K. In order to avoid oxidation during heating, each sample was put in a quartz tube, sealed under vacuum and heated for 60 min at each temperature being tested.

The diffraction pattern of the as-prepared alloy (cf. Fig. 2) shows only a very broad peak in the 2θ range between 40° and 50° without appreciable diffraction peaks corresponding to crystalline phases, thus indicating the absence of any long-range crystalline order, as is characteristic for an amorphous structure. This pattern remained almost unchanged after annealing at 573 and 713 K.

Table 1
Kinetic parameters for both observed crystallization stages.

β (K/min)	First stage			Second stage		
	T_p^1(K)	E_a^1(kJ/mol)	$\ln A^1$ (A [min^{-1}])	T_p^2(K)	E_a^2(kJ/mol)	$\ln A^2$ (A [min^{-1}])
5	796.5	486.3 ± 8	72.7		439.3 ± 8	63.7
10	802.9	(Kissinger)	(Kissinger)	839.6	(Kissinger)	(Kissinger)
20	811.9	499.9 ± 8	88.1	847.9	460.8 ± 8	79.2
40	819.0	(Ozawa)	(Ozawa)	857.5	(Ozawa)	(Ozawa)

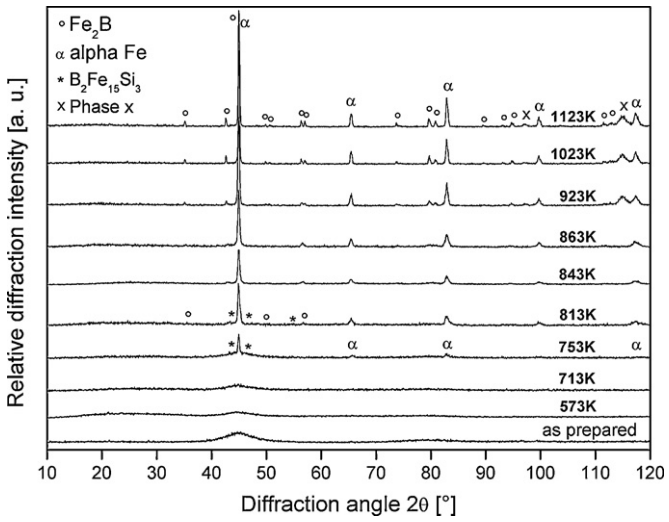

Fig. 2. XRD patterns of the as-prepared $Fe_{89.8}Ni_{1.5}Si_{5.2}B_3C_{0.5}$ alloy as well as corresponding samples heated for 60 min at different temperatures at 573, 713, 753, 813, 843, 863, 923, 1023 and 1123 K.

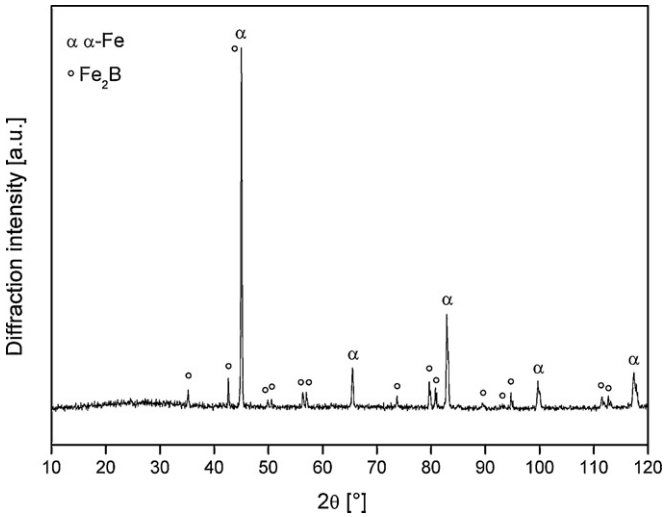

Fig. 3. XRD pattern of the sample heated at a temperature of 1123 K for 7 h.

The results presented in Fig. 2 indicate that different structural transformations of the alloy occurred in the temperature range 753–1123 K. Initially at 753 K the presence of the α-iron phase (ICDD-PDF 00-036-4899) as the major phase and the boron–iron–silicon phase, $B_2Fe_{15}Si_3$ (ICDD-PDF 00-047-1629), was observed. The boron–iron–silicon phase was present only in very small amounts in the temperature range from 753 to the 813 K. The next step in the structural transformations induced by thermal treatment was formation of the iron–boron phase, Fe_2B (ICDD-PDF 00-036-1332), observed for 813 K. The iron–boron phase coexisted with the α-iron phase over the whole range of temperatures from 813 to 1123 K. Further heating above 813 K did not affect significantly the phase composition until a temperature of 923 K, when besides the α-iron and iron–boron phase, two reflexions at the diffraction angles 97.122° and 114.886° indicate the presence of one new intermediate phase, presented in Fig. 2 as phase x. Due to the restriction of many ICDD-PDF data entries to a lower 2θ range and since adequate peaks at lower diffraction angles could not be observed, complete identification of this phase was not possible. However, the diffraction pattern corresponds well to a supposed phase with cubic symmetry (face-centered structure).

Fig. 3 shows the XRD pattern of the sample held for 7 h at a temperature of 1123 K. After this heating only the α-Fe and Fe_2B phases were present and no intermediate phase occurred. These results have a good correlation with previously mentioned DSC results where it was shown that two crystallization peaks indicate a multi-stage crystallization process of the alloy.

The Rietveld refinement method [27] was used for the determination of the weight fraction of the crystalline phases that were formed and of the amorphous content as well. As shown in Fig. 4, the content of the boron–iron–silicon phase ($B_2Fe_{15}Si_3$) observed at 753 K decreased and at 843 K this phase disappeared completely. In the same time, the relative phase contribution of the α-Fe phase increased almost linearly (taking the amorphous content into account), while the weight fraction of the iron–boron (Fe_2B) phase increased slightly.

On raising the temperature an increasing weight content of crystalline phases (cf. Fig. 4) was expected but the broad maximum from a residual amorphous phase at small diffraction angles as well as for the diffraction angle range of 40–50° indicates that the heating caused only a partial crystallization of the sample. For the final heat treatment (1 h) at a temperature of 1123 K, slightly less than 4% of the amorphous fraction still remained.

The Rietveld refinement method also gave the phase weight fraction values for the final diffraction pattern corresponding to the sample heated at 1123 K for 7 h (cf. Fig. 3). The results (61 wt.% of the α-Fe phase, 39 wt.% Fe_2B phase, and no amorphous phase present) indicate a significant alteration in the phase composition due to heating of alloy. These final contents are most likely near the thermal equilibrium.

Besides the temperature dependence of the crystalline fraction, the lattice constants for the Fe_2B iron-boron phase, Fig. 5, show the temperature dependence but not the lattice constant for the cubic α-Fe phase. The lattice constants as well as the Hermann–Mauguin space group symbol for all observed phases corresponding to the ICDD-PDF data are presented in Table 2.

The diagram presented in Fig. 5 shows clearly that the lattice constant a for the Fe_2B phase increased from 5.095 Å at 813 K to 5.102 Å at 1123 K reaching the maximal value of 5.141 Å at a temperature of 863 K. The lattice constant c increased continuously from 4.180 to 4.252 Å over this temperature range. These changes correspond to structural and stoichiometric variations of the boride phase during the formation reaction. This effect is mainly caused by reactions between the coexisting phases. Furthermore, the deviation from the theoretical values as given in Table 2 is caused by

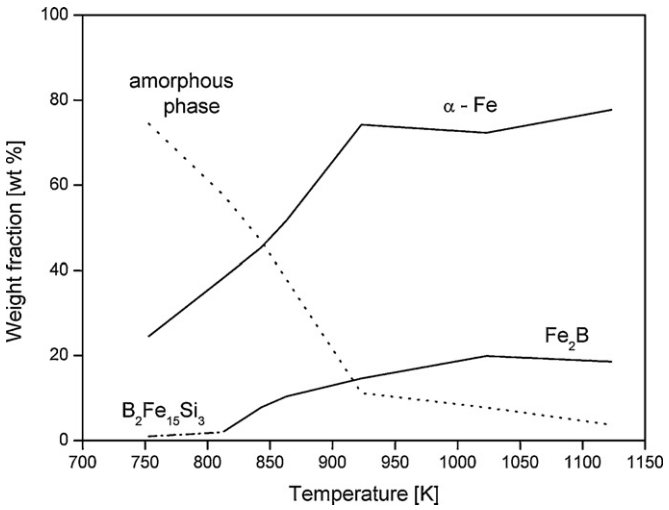

Fig. 4. Weight fractions of the observed crystalline phases as obtained by Rietveld refinement including the obtained amorphous weight content, plotted as a function of the heating temperature (1 h).

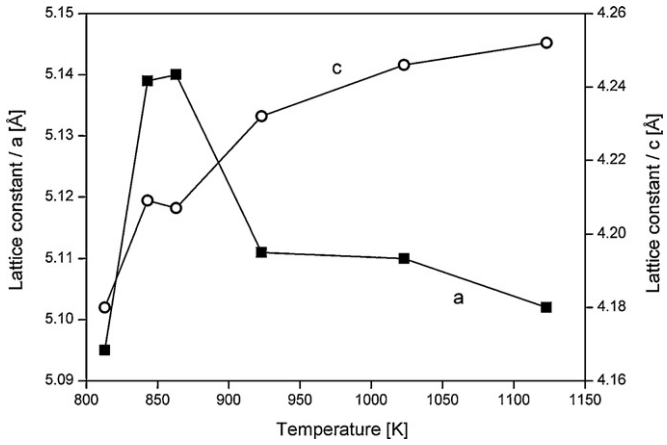

Fig. 5. Lattice constants *a* (indicated by squares) and *c* (indicated by circles) of the Fe_2B phase as obtained by Rietveld refinement procedure plotted as a function of the heating temperature.

Table 2
The lattice constants as well as the Hermann–Mauguin space group symbol for all observed phases according to the ICDD-PDF database.

Phase	Formula	Space group	Crystal system	Lattice parameters (Å)	
				a	*c*
α-Iron	Fe	*Im*-3*m*	Cubic	2.867	–
Iron–boron	Fe_2B	*I*4/*mcm*	Tetragonal	5.110	4.249
Boron–iron–silicon	$B_2Fe_{15}Si_3$	*I*-4	Tetragonal	8.677	4.307

the additional incorporation of the remaining elements (i.e. Si, C, and Ni). It could be shown that the crystal growth is temperature dependent (cf. Fig. 6). The crystallization process for the major α-Fe phase as well as for the Fe_2B phase with the smallest average crystallite sizes interpreted from the XRD data were in the range from 16 to 29 nm. With increasing temperature the average crystallite size reached a maximum value between 101 and 119 nm at 1123 K (cf. Table 3).

The surface of the samples before and after heat treatment was inspected by a scanning electron microscopy (cf. Figs. 7 and 8) in order to correlate the results of the XRD phase analysis with changes in the sample surface microstructure. To obtain a surface suitable for accurate particle shape and size observation the samples were subjected to specific preparation procedure. Considering the small dimensions (around $3 \times 2 \times 0.5$ mm) it was necessary to embed each sample in a conductive hot resin based on iron powder. Subsequently the sample was smoothed with 500, 1200, 2400, and finally 4000 grit grinding silicon carbide (SiC) paper. The sample surface was then polished with a diamond emulsion with 3 and 1 μm grain sizes. The final polishing step was conducted with a 40 nm colloidal silica solution.

In Fig. 7 the SEM micrographs are shown for as-prepared and the thermally treated alloy samples. From Fig. 7a which shows the surface of as-prepared alloy it is obvious that the amorphous surface is completely homogeneous. The heat treatment leads to crystalline phase formation and the formation of a non-homogeneous surface of the alloy. For the temperature of 753 K where the first presence of a crystalline phase was observed, the first partial surface non-homogeneity was observed as well. Fig. 7b shows the existence of surface fractures for a sample heated at 753 K. Further heating at higher temperatures increased the surface non-homogeneity as is shown in Fig. 7c for a sample thermally treated at 923 K for 1 h.

However, the presence of twinning and crystal lattice deformations such as dislocations accompany the overall heating procedure. Fig. 8 indicates the presence of twins (sample heated at 1123 K for 60 min). This SEM micrograph shows the presence of grain structure of two different phases in a sample heated at 1123 K for 7 h, that is in good accordance with X-ray data. The larger particles with a grain size in a range of 1–3 μm probably correspond to the Fe_2B phase and the smaller particles with a grain size in a range of 0.5–1 μm are related to the α-Fe phase. These values are slightly larger than the dimensions we obtained from the X-ray diffraction pattern in Table 3. This difference is due to the mechanism of XRD which is strictly related to the smaller coherent diffracting length [15]. The smallest, white, globular shaped particles in Fig. 8 occur only in traces, probably corresponding to residuals from the final fine polishing; the particle size of approximately 40 nm corresponds to the grain size of colloidal polishing silica solution. Additionally, in Fig. 9, the SEM micrograph of the fracture surface of the sample (cross-section, same sample as in Fig. 8) is also displayed. Here the globular shaped particles were not observed.

As expected, an increased crystallinity of the material correlates with a decrease of the hardness (cf. Fig. 10). The structural transformations which give rise to a more pronounced sam-

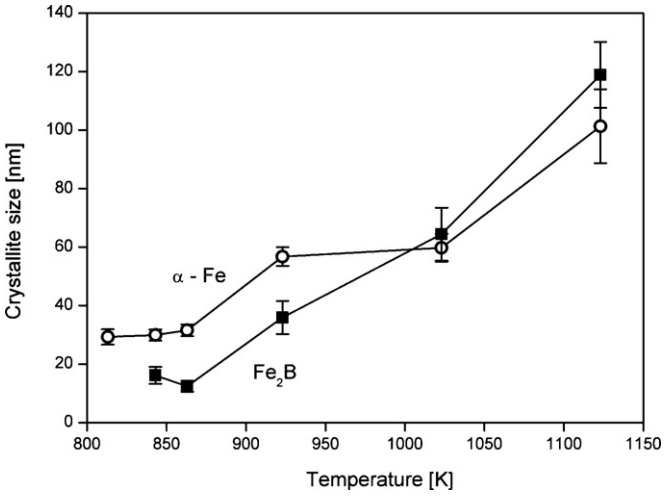

Fig. 6. Crystallite size as deduced from Rietveld refinement data for the α-Fe and Fe_2B phases plotted as a function of the heating temperature.

Table 3
Overview of crystallite size D_{hkl}, dislocation density ρ_{hkl} and microstrain ε_{hkl} of the samples heated at different temperatures.

Temperature (K)	Heating time (h)	Fe_2B		α-Fe		ε_{hkl} (%)
		D_{hk} (nm)	ρ_{hkl} (m^{-2})	D_{hkl} (nm)	ρ_{hkl} (m^{-2})	
813	1	–	–	29	3.57×10^{15}	12.81
843	1	16	1.17×10^{16}	30	3.33×10^{15}	10.57
863	1	12	2.08×10^{16}	32	2.93×10^{15}	9.72
923	1	36	2.31×10^{15}	57	9.23×10^{14}	4.97
1023	1	64	7.32×10^{14}	60	8.33×10^{14}	5.55
1123	1	119	2.12×10^{14}	101	2.94×10^{14}	2.73
1123	7	178	9.47×10^{13}	123	1.98×10^{14}	1.78

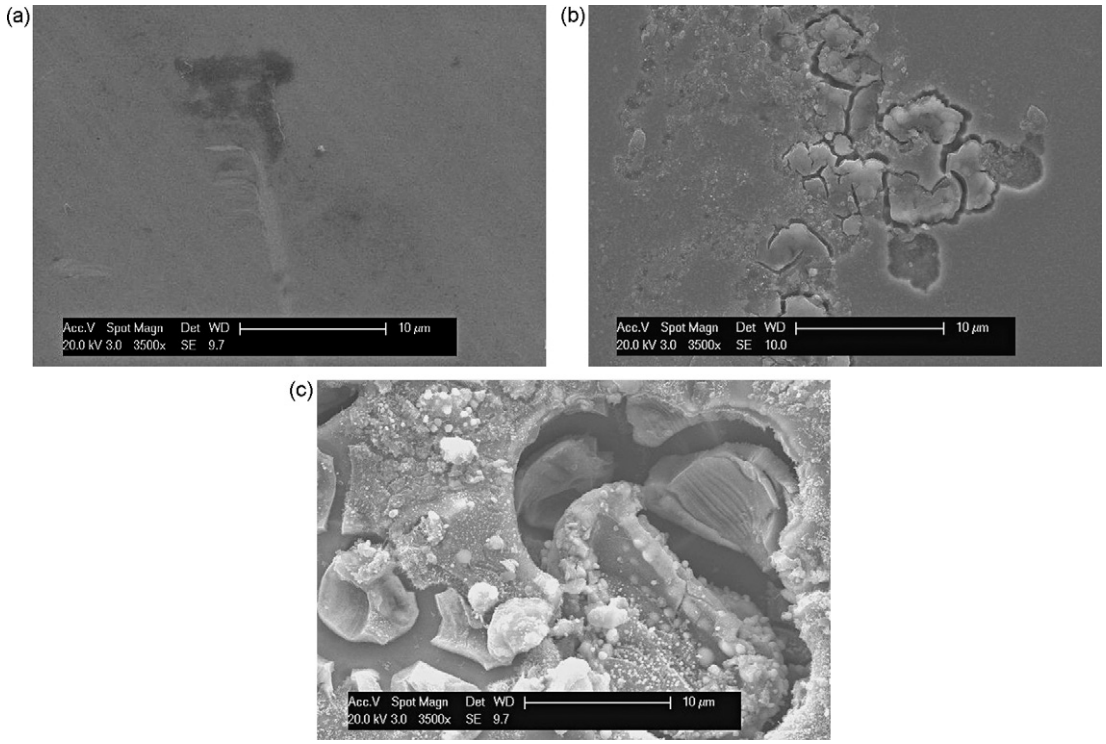

Fig. 7. (a) Scanning electron micrographs of the sample surfaces – as-prepared. (b) Scanning electron micrographs of the sample surfaces – after heat treatment at 753 K. (c) Scanning electron micrographs of the sample surfaces – after 923 K for 60 min.

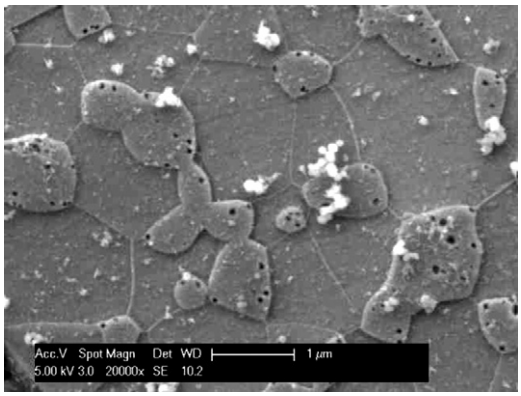

Fig. 8. Scanning electron micrograph of the polished surface of a $Fe_{89.8}Ni_{1.5}Si_{5.2}B_3C_{0.5}$ sample heated at 1123 K for 7 h.

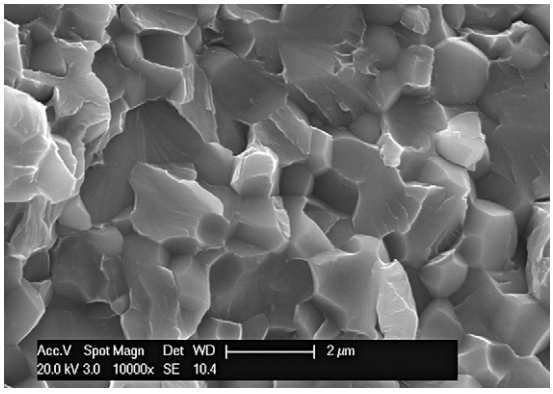

Fig. 9. Scanning electron micrograph of the cross-section (fracture surface) of a $Fe_{89.8}Ni_{1.5}Si_{5.2}B_3C_{0.5}$ sample heated at 1123 K for 7 h.

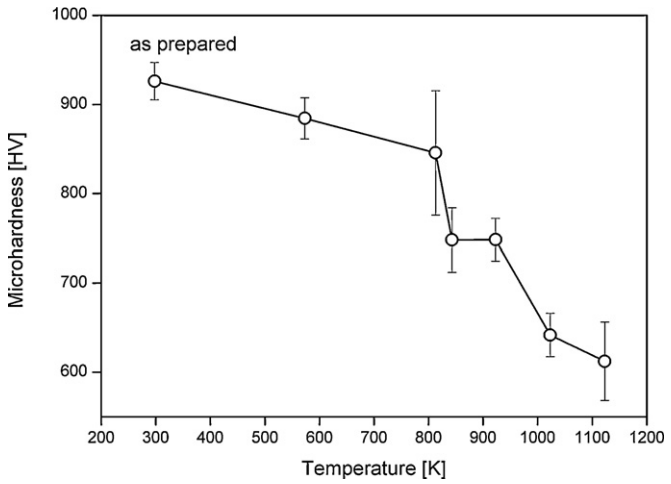

Fig. 10. Vickers microhardness (HV) mean values of the samples plotted as a function of the heating temperature together with the standard deviation error bars.

ple non-homogeneity most likely induce higher variations of the microhardness (cf. the error bars in Fig. 10).

4. Conclusions

As can be seen from the results, the $Fe_{89.8}Ni_{1.5}Si_{5.2}B_3C_{0.5}$ amorphous alloy was stable up to a temperature of 753 K when structural transformations began. This process started with formation of the α-Fe phase, which was followed by formation of the Fe_2B phase at temperatures above 813 K. Up to a temperature of 863 K, the crystallite size remained almost constant, while at higher temperatures a significant crystal growth occurred. This observation can most likely be explained by the assumption of two recrystallization phases: in a first step the number of crystallites (seeds) grew. Each of these particles displayed almost constant size. In a second step

a certain fraction of the crystallites grew by consumption of the smaller particles. During this process (especially above 923 K) the total crystalline volume remained almost unchanged. The observed weight fraction of the crystalline α-Fe phase increased up to 923 K while in the higher temperature range an almost constant content was achieved. The Fe_2B phase shows no such expressed behavior.

Acknowledgements

The authors want to thank Dr. J. Wosik for his helpful assistance concerning the SEM investigations and Dr. N. Krendelsberger for her support in the heating experiments.

The investigation was partially supported by the Ministry of Science and Environmental Protection of Serbia, the Project 142025. The work at CEST was supported within the COMET program by the Austrian Research Promotion Agency (Österreichische Forschungsförderungsgesellschaft, FFG) and the government of Lower Austria.

References

[1] R.A. Cowley, C. Patterson, N. Cowlam, P.K. Ivison, J. Martinez, L.D. Cussen, J. Phys.: Condens. Matter 3 (1991) 9521.
[2] U. Köster, U. Herald, Crystallisation of Metallic Glasses in Topics of Applied Physics, vol. 46, Springer, New York, 1981, p. 225.
[3] M. Iqbal, J.I. Akhter, H.F. Zhang, Z.Q. Hu, J. Non-Cryst. Solids 354 (2008) 5363.
[4] Y. Wu, X.D. Hui, Z.Y. Liu, L. Liang, G.l. Chen, J. Alloys Compd. 467 (2009) 187.
[5] M. Miglierini, J. Non-Cryst. Solids 354 (2008) 5093.
[6] H. Beniani, J.S. Blazquez, C.F. Conde, A. Conde, J. Alloys Compd. 454 (2008) 156.
[7] D.S. Santos, D.R. dos Santos, J. Non-Cryst. Solids 304 (2002) 56.
[8] N. Bayri, T. Izgi, H. Gencer, P. Sovak, M. Gunes, S. Atalay, J. Non-Cryst. Solids 355 (2009) 12.
[9] A. Hsiao, M.E. McHenry, D.E. Laughlin, M.J. Kramer, C. Ashe, T. Ohkubo, IEEE Trans. Magn. 38 (5) (2002) 3039.
[10] S.W. Du, R.V. Ramanujan, J. Non-Cryst. Solids 351 (2005) 3105.
[11] S. Li, S. Bai, H. Zhang, K. Chen, J. Xiao, J. Alloys Compd. 470 (2009) 141.
[12] D.S. Santos, R.S. Biasi, J. Alloys Compd. 335 (2002) 266.
[13] J. Bonastre, L. Escoda, J. Saurina, J.J. Sunol, J.D. Santos, M.L. Sanchez, B. Hernado, J. Non-Cryst. Solids 354 (2008) 5126.
[14] J. Vasquez, P.L. Lopez-Alemany, P. Villares, R. Jimenez-Garay, J. Alloys Compd. 61 (2000) 493.
[15] D.R. Santos, I.L. Torriani, A.Y. Ramos, M. Knobel, J. Appl. Crystallogr. 30 (1970) 633.
[16] G.A. Jones, P. Bonnett, S.F.H. Parker, J. Magn. Magn. Mater. 58 (1986) 216.
[17] N. Saegusa, A.H. Morrish, Phys. Rev. B26 (1982) 305.
[18] D.M. Minić, A. Maričić, A.R. Dimitrijević, M.M. Ristić, J. Alloys Compd. 430 (2007) 430.
[19] D.M. Minić, A. Maričić, B. Adnadjević, J. Alloys Compd. 473 (2009) 363.
[20] D.M. Minić, A. Gavrilović, P. Angerer, D.G. Minić, A. Maričić, J. Alloys Compd 476 (2009) 706.
[21] D.M. Minić, B. Adnadjević, Thermochim. Acta 424 (2008) 41.
[22] Bruker AXS, TOPAS V3. General profile and structure analysis software for powder diffraction data, Karlsruhe, 2005.
[23] H.E. Kissinger, Anal. Chem. 29 (1957) 1702.
[24] T. Ozawa, J. Therm. Anal. 29 (1970) 301.
[25] S.D. Kaloshkin, I.A. Tomilin, Thermochim. Acta 280–281 (1996) 303.
[26] K.G. Raval, K.N. Lad, A. Pratap, A.M. Awasthi, S. Bhardwaj, Thermochim. Acta 425 (2005) 47.
[27] L.B. McCusker, R.B. Von Dreele, D.E. Cox, D. Louër, P. Scardi, J. Appl. Crystallogr. 36 (1999) 32.